Charge Radii of Neutron Deficient ^{52,53}Fe Produced by Projectile Fragmentation

K. Minamisono,[1,2] D. M. Rossi,[3] R. Beerwerth,[4,5] S. Fritzsche,[4,5] D. Garand,[1] A. Klose,[6] Y. Liu,[7] B. Maaß,[3] P. F. Mantica,[8,9] A. J. Miller,[1,2] P. Müller,[10] W. Nazarewicz,[8,2,11] W. Nörtershäuser,[3] E. Olsen,[1] M. R. Pearson,[12] P.-G. Reinhard,[13] E. E. Saperstein,[14,15] C. Sumithrarachchi,[1] and S. V. Tolokonnikov[14,16]

[1]*National Superconducting Cyclotron Laboratory, Michigan State University, East Lansing, Michigan 48824, USA*
[2]*Department of Physics and Astronomy, Michigan State University, East Lansing, Michigan 48824, USA*
[3]*Institut für Kernphysik, Technische Universität Darmstadt, 64289 Darmstadt, Germany*
[4]*Helmholtz-Institut Jena, Jena 07743, Germany*
[5]*Theoretisch-Physikalisches Institut, Friedrich-Schiller-Universität Jena, 07743 Jena, Germany*
[6]*Department of Chemistry, Augustana University, Sioux Falls, South Dakota 57197, USA*
[7]*Physics Division, Oak Ridge National Laboratory, Oak Ridge, Tennessee 37831, USA*
[8]*Facility for Rare Isotope Beams, Michigan State University, East Lansing, Michigan 48824, USA*
[9]*Department of Chemistry, Michigan State University, East Lansing, Michigan 48824, USA*
[10]*Physics Division, Argonne National Laboratory, Lemont, Illinois 60439, USA*
[11]*Institute of Theoretical Physics, Faculty of Physics, University of Warsaw, 02-093 Warsaw, Poland*
[12]*TRIUMF, Vancouver, British Columbia V6T 2A3, Canada*
[13]*Institut für Theoretische Physik, Universität Erlangen, D-91054 Erlangen, Germany*
[14]*National Research Centre "Kurchatov Institute," 123182 Moscow, Russia*
[15]*National Research Nuclear University MEPhI, 115409 Moscow, Russia*
[16]*Moscow Institute of Physics and Technology, 141700 Dolgoprudny, Russia*

(Received 5 October 2016; revised manuscript received 4 November 2016; published 15 December 2016)

Bunched-beam collinear laser spectroscopy is performed on neutron deficient ^{52,53}Fe prepared through in-flight separation followed by a gas stopping. This novel scheme is a major step to reach nuclides far from the stability line in laser spectroscopy. Differential mean-square charge radii $\delta\langle r^2\rangle$ of ^{52,53}Fe are determined relative to stable ^{56}Fe as $\delta\langle r^2\rangle^{56,52} = -0.034(13)$ fm^2 and $\delta\langle r^2\rangle^{56,53} = -0.218(13)$ fm^2, respectively, from the isotope shift of atomic hyperfine structures. The multiconfiguration Dirac-Fock method is used to calculate atomic factors to deduce $\delta\langle r^2\rangle$. The values of $\delta\langle r^2\rangle$ exhibit a minimum at the $N = 28$ neutron shell closure. The nuclear density functional theory with Fayans and Skyrme energy density functionals is used to interpret the data. The trend of $\delta\langle r^2\rangle$ along the Fe isotopic chain results from an interplay between single-particle shell structure, pairing, and polarization effects and provides important data for understanding the intricate trend in the $\delta\langle r^2\rangle$ of closed-shell Ca isotopes.

DOI: 10.1103/PhysRevLett.117.252501

Introduction.—Since the first estimate of a nuclear charge radius in 1909 [1,2], the size of a nucleus has been a central theme in nuclear structure [3–7]. Significant data on charge radii have been obtained at isotope separator on line (ISOL) facilities, where isotopes of selective elements have been investigated. The ISOL production method, however, suffers from a serious limitation due to long release times from thick targets. This can lead to large decay losses for nuclides that have long diffusion and/or effusion times and with short half-lives at the limits of the nuclear chart. In-flight production and separation [8] used in the present study can provide high-energy fast beams and enable studies on nuclides far from the stability line and elements that are difficult at ISOL facilities. Conversion of the fast beams into low-energy beams in a gas [9] was already exploited and was used for laser spectroscopy for the first time in the present study on transition-metal Fe known to be notoriously difficult to produce at ISOL facilities. This is a major step forward for laser spectroscopy experiments that complements such capabilities already well established at ISOL facilities.

The average behavior of nuclear root-mean-square (rms) charge radii approximately follows the liquid-drop relation $\sqrt{\langle r^2\rangle} \propto A^{1/3}$ with A being the mass number. The measured radii display local variations around the average trend, which signal various nuclear structure effects; a kink in an isotopic chain of rms charge radii at nucleonic shell closures is one such feature [10]. The underlying structural mechanism behind this discontinuity still remains elusive and even might vary for different shell closures. The possible explanations range from shifts of nucleonic shells due to the spin-orbit potential [11], beyond mean-field correlation effects due to zero-point fluctuations [12] and configuration mixing [13], changes in shell occupations [14,15], and density-dependent spin-orbit potentials [16,17]. Another subtle feature is the odd-even staggering with A, which has been explained [18] in terms of the density-dependent pairing interaction. Both features are clearly visible in the Ca chain, and it has been a

major challenge for nuclear theory to understand the intricate pattern. In particular, the almost equal values of ^{40}Ca and ^{48}Ca radii with eight more neutrons added was discussed in terms of the novel density dependence of energy density functionals [17–19] and recently reproduced by *ab initio* coupled cluster calculations with optimized two- and three-body interactions [20,21].

Regardless of the actual mechanism, trends in rms charge radii carry extremely valuable information on nuclear interactions and many-body nucleonic dynamics. The main objective of the present study is to investigate how the pattern of rms charge radii around $N = 28$ changes when moving from semimagic Ca isotopes to Fe isotopes, where the neutron-proton polarization effects are stronger. The charge radii of neutron deficient ^{52,53}Fe below the $N = 28$ neutron-shell closure were determined, which is the heaviest element that crosses $N = 28$ after Mn isotopes [22], where a kink similar to Ca was observed. The results are discussed within the framework of the self-consistent nuclear density functional theory.

Experiment.—The experiment was performed at the National Superconducting Cyclotron Laboratory at Michigan State University. The radioactive ^{52}Fe ($T_{1/2} = 8.28$ h, $I^\pi = 0^+$) and ^{53}Fe (8.52 m, $7/2^-$) ion beams were produced by fragmentation of a 160-MeV/nucleon ^{58}Ni beam in a Be target. The ^{52}Fe or ^{53}Fe beams were selected through the A1900 fragment separator [8], thermalized in a gas stopper [9], and extracted as singly charged ions at an energy of 30 keV. The Fe^+ beam was transported to the beam cooler and laser spectroscopy (BECOLA) facility [23,24], where the beam was injected into a radio frequency quadrupole cooler and buncher [25]. The trapped ion beam was extracted at an energy of 29 856(4) V as ion bunches for the bunched-beam collinear laser spectroscopy [26,27]. A charge-exchange cell [28,29] containing sodium vapor was used to neutralize the incoming Fe^+ beam for laser-induced fluorescence measurements on the $3d^64s^2{}^5D_4 \leftrightarrow 3d^64s4p^5{}^5F_5$ transition in Fe I at 372 nm [30]. A Sirah Matisse TS Ti:sapphire ring laser was used to produce 744 nm light. A Spectra Physics wave train generated 372 nm light by frequency doubling the 744 nm light.

Ion beams of stable ^{56}Fe were produced using a Penning ionization gauge ion source [29]. The ^{56}Fe beam was introduced into the BECOLA beam line every several hours throughout the experiment, and hyperfine spectra were measured as a reference to determine the isotope shifts and to monitor the time-dependent centroid shift.

Experimental results.—The hyperfine spectra of ^{52,53}Fe and the reference ^{56}Fe are shown in Fig. 1. The reduced chi squares of the fits were $\chi^2/\nu = 1.06$ and 1.00 for ^{52}Fe and ^{53}Fe, respectively. Isomeric states of Fe were present in the beam but did not affect the measurements due to their small production fractions to the ground state of 0.30(1)% and 5.0(2)% for ^{52}Fe and ^{53}Fe, respectively. The isotope shifts were obtained as $\delta\nu^{56,52} = -1.839(3)(6)$ GHz and $\delta\nu^{56,53} = -1.252(4)(5)$ GHz, where the first and second parentheses are the statistical and systematic errors, respectively. The systematic error is dominated by the uncertainty of 11 V of the potential, at which the ions were released from the cooler and buncher.

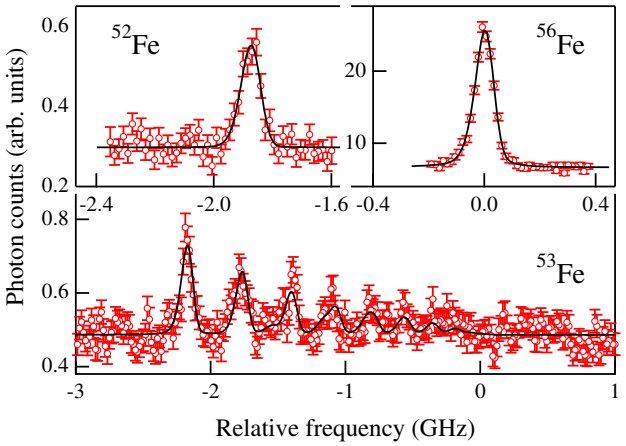

FIG. 1. Hyperfine spectra of ^{52,53,56}Fe. The open circles are the data, and the solid lines are best fits of an asymmetric Voigt profile [28,31] to the data.

The differential mean-square (ms) charge radius $\delta\langle r^2\rangle^{A,A'} = \langle r^2\rangle^{A'} - \langle r^2\rangle^{A}$ can be obtained from the isotope shift of atomic hyperfine structures between isotopes A and A' with k and $F_{\rm el}$ being the mass and field shift coefficients, respectively, and m the atomic mass:

$$\delta\nu^{A,A'} = \nu^{A'} - \nu^{A} = k\frac{m_{A'} - m_A}{m_{A'}m_A} + F_{\rm el}\delta\langle r^2\rangle^{A,A'}. \quad (1)$$

Here $k = k_{\rm NMS} + k_{\rm SMS}$ with $k_{\rm NMS} = \nu m_e$, where $k_{\rm NMS}$ and $k_{\rm SMS}$ are the normal and specific mass shift coefficients, respectively, ν is the transition frequency of the reference isotope, and m_e is the electron mass. The k and $F_{\rm el}$ were computed using the multiconfiguration Dirac-Fock (MCDF) method [32] as implemented in the GRASP2k package [33]. The relativistic isotope shift (RIS3) module [34] was utilized to compute k, while $F_{\rm el}$ was calculated by a procedure described in Refs. [35,36]. The results of these calculations are summarized in Table I. Model I is a

TABLE I. k (GHz amu) and $F_{\rm el}$ (GHz/fm^2) calculated by the MCDF method for the $^5D_4 \rightarrow {}^5F_5$ transition in Fe I. ΔE (cm^{-1}) is the transition energy, and CSF is the number of basis functions.

	ΔE	$k_{\rm NMS}$	$k_{\rm SMS}$	$F_{\rm el}$	CSF
Model I	24 805	318	438	−0.55	466 254
Model II	26 462	279	776	−0.52	700 531
Model III	26 392	294	746	−0.52	752 942
Exp. [37]	26 874.55	441.97	950(140)	−0.60(31)	
Theory [38]			734		
Adopted		441.97	911(43)	−0.52(8)	

single-reference calculation, where the wave-function expansion in terms of configuration-state functions is generated by virtual single and double excitations from the ground configuration $3d^6 4s^2$ and the excited configuration $3d^6 4s 4p$ into several layers of correlation orbitals with $\ell \leq 4$. Since the result is clearly unbalanced as ΔE is significantly too low, model II was constructed with a multireference set that also contains $3d^6 4p^2$ and $3d^7 4p$ in addition to the ground and excited levels, respectively. Computational limitations permitted three correlation layers. A fourth correlation layer was added in model III by limiting $\ell \leq 3$. Since the fourth layer has a negligible impact on the results, a good convergence with respect to the valence-valence correlation was confirmed.

The F_{el} is slightly lowered by the multireference set and in good agreement with the experimental value [37], which has a 50% uncertainty. Since the open d shell did not permit an accurate accounting for core-correlation effects, the effect of core polarization was estimated in a series of calculations with purely single excitations from the Ar core. This resulted in a variation of $\sim$0.02 GHz/fm^2 on F_{el}. The F_{el} was finally determined to be $F_{\mathrm{el}} = -0.52(8)$ GHz/fm^2, where a 15% error was conservatively assumed for the remaining neglected correlation with the core. The k is much more sensitive to correlation effects and changes drastically in the multireference models (II and III), as compared to the first single-reference computation, and also smaller than the experimental value [37]. Alternatively, the k may be evaluated using the King plot analysis [39] with the $\delta\langle r^2\rangle$ of stable isotopes evaluated from electron-scattering and muonic-atom experiments [40] and the $\delta\nu^{A,A'}$ [37] of the transition used in the present work. A linear regression analysis was performed with the slope fixed to the calculated value of F_{el} and both uncertainties of $\delta\langle r^2\rangle$ and $\delta\nu$ being considered, where the systematic uncertainties of the Barrett radii [41] were also taken into account. The obtained semiempirical value of $k = 1353(43)$ GHz amu together with the calculated F_{el} result in $\delta\langle r^2\rangle^{56,52} = -0.034(13)(110)$ fm^2 and $\delta\langle r^2\rangle^{56,53} = -0.218(13)(91)$ fm^2, which are summarized in Table II. Here the first and second errors are the quadratic sum of the statistical and systematic errors on $\delta\nu^{56,A}$ and uncertainties on the atomic factors, respectively.

TABLE II. $\delta\langle r^2\rangle$ (fm^2) for $^{52-58}$Fe isotopes. The $\delta\langle r^2\rangle^{54,A}$ of this work is obtained using the $\delta\langle r^2\rangle^{56,54}$ [40].

A	$\delta\langle r^2\rangle^{56,A}$	$\delta\langle r^2\rangle^{54,A}$	References
52	−0.034(13)(110)	0.282(14)(73)	This work
53	−0.218(13)(91)	0.097(14)(35)	This work
54	−0.316(5)	0.00	[40]
56	0.00	0.316(5)	[40]
57	0.125(6)	0.441(6)	[40]
58	0.285(6)	0.601(6)	[40]

Density functional theory models.—The rms charge radii of Fe and Ca isotopes were predicted by means of the nuclear density functional theory (DFT) [42], which is particularly well suited for the microscopic description of complex nuclei. At the heart of the nuclear DFT lies the energy density functional (EDF) that characterizes the effective interactions between nucleons; the coupling constants of the EDF are usually adjusted to experimental data, including rms charge radii and binding energies [42–45]. The rms charge radii were calculated from self-consistent proton densities corrected by proton and neutron form factors and spin-orbit contributions.

Two Skyrme EDFs, SV-min [43] and UNEDF0 [44], as well as two Fayans EDFs, FaNDF^0 [45] and DF3-a [19], were used. The Skyrme EDFs contain all conceivable bilinear couplings of densities and currents up to second order in derivatives, and the corresponding density-dependent pairing functional is of the mixed type [46]. Fayans EDFs have a more complex dependence on particle densities that stems from a fractional form of their density-dependent couplings and contain a Coulomb-nuclear correlation term. The pairing functional of Fayans EDFs effectively accounts for the coupling to surface vibrations and contains the novel density-gradient term, which is essential for explaining the odd-even staggering in rms charge radii [18]. The coupling constants of the pairing functional were adjusted to one-neutron separation energies of the specific isotopic chain, and other coupling constants, determined from fits to ground-state properties of magic nuclei, were common to both Ca and Fe.

Since zero-point quadrupole fluctuations, important for transitional nuclei, are missing in Skyrme EDFs, quadrupole correlations were considered. This was done in the framework of the multireference DFT at the level of the Gaussian-overlap approximation [47,48]. The Fayans calculations were carried out under the assumption of a spherical nuclear shape. Blocking calculations for odd-A systems were performed by means of the standard uniform filling approximation.

Discussion.—The measured and predicted values of charge radii along the isotopic chains of Fe and Ca and neighboring isotopes are shown in Fig. 2. An appreciable minimum at $N = 28$ can be identified in the experimental rms charge radii for Fe with the addition of new data on ^{52,53}Fe, and the values of $\delta\langle r^2\rangle^{54,52}$ and $\delta\langle r^2\rangle^{54,56}$ are similar. The Ca chain exhibits a parabolic behavior with a strong odd-even staggering between the almost identical values of ^{40}Ca and ^{48}Ca. Above ^{48}Ca, experimental rms charge radii increase rapidly, reaching a large value at ^{52}Ca, which is difficult to explain in the microscopic theory [21]. Above $N = 28$, K [51], Cr [40], and Mn [22] chains show a trend similar to the Ca chain. However, the Mn and Fe chains have similar values at $N = 26$ showing a rapid increase also below $N = 28$, which deviates from the

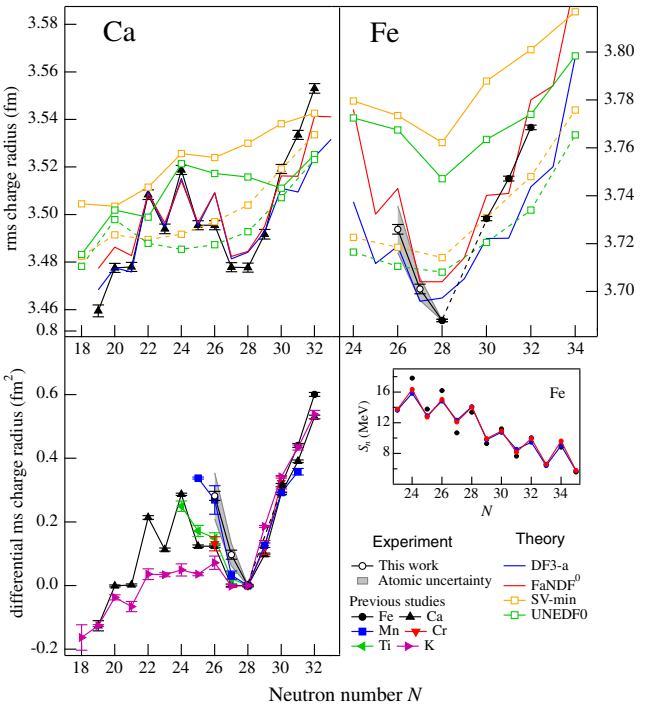

FIG. 2. rms charge radii (top) of the isotopic chains of Ca (left) and Fe (right) and differential ms charge radii (bottom) of K-Fe (left). Data are taken from Refs. [21,22,40,49–51], and this work. The uncertainties in the atomic factors are marked by shading. Calculations with SV-min and UNEDF0 EDFs were performed for even-even mass isotopes only. The inset shows one-neutron separation energies for the Fe chain.

Ca trend. The large Fe radius at $N = 27$ indicates a smaller odd-even staggering effect in the Fe chain.

The predictions of single-reference DFT calculations with UNEDF0 and SV-min for the Ca chain, shown in Fig. 2 by dashed lines, are typical of Skyrme functionals that have been calibrated to experimental rms charge radii: They overestimate the rms charge radii for both ^{40}Ca and ^{48}Ca and are unable to reproduce either the kink at $N = 28$ or the local maximum at ^{44}Ca [15,21]. The situation around ^{44}Ca is only slightly improved when quadrupole correlations are added (solid lines), but the pattern in neutron-rich Ca isotopes deteriorates [21]. Fayans-DFT calculations of the Ca chain for both FaNDF^0 and DF3-a reproduce the experimental rms charge radii well, including the odd-even staggering [18,19]. While the value of $\delta\langle r^2\rangle^{48,52}$ is still underestimated, the overall trend is predicted correctly.

The single-reference Skyrme-DFT calculations with UNEDF0 and SV-min for the Fe chain (dashed lines) predict a minimum at $N = 28$, but the kink is not as pronounced as the one in the experimental data. A more prominent kink is obtained when quadrupole correlations are added (solid lines). The reason for this is given in Fig. 3, which shows that the considered Fe isotopes are predicted to be quadrupole soft, and ^{52}Fe is even expected to be deformed (also see the experimental evidence [52]) with the

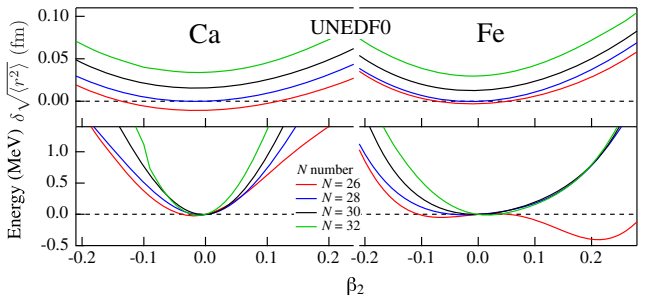

FIG. 3. rms charge radii (top) plotted relative to $\sqrt{\langle r^2\rangle}$ at $N = 28$; $\beta_2 = 0$, and potential energies (bottom) for the Ca (left) and Fe (right) chains calculated with UNEDF0 as a function of β_2. Results with SV-min (not shown) are similar.

quadrupole deformation parameter of $\beta_2 \sim 0.22$. Since the calculated rms charge radii of ^{52}Fe and ^{54}Fe are very similar around the spherical shape, larger quadrupole correlations in ^{52}Fe impact its rms charge radii. The predicted value of ^{52}Fe at the deformed minimum is as large as that of ^{56}Fe and agrees with the experimental trend. On the other hand, the Ca isotopes, which are predicted to be spherical and more rigid with respect to deformation, show a monotonic increase of rms charge radii with N. Therefore, the deformation effect alone cannot account for the large value of $\delta\langle r^2\rangle^{48,46}$ seen in the experiment.

Though the odd-even staggering in the Fe chain is overestimated, the general agreement between the Fayans EDFs and experiments is very good for both isotopic chains. One can shed new light on this superior performance of the Fayans EDFs over the Skyrme EDFs by comparing their predictions for separation energies in ^{48}Ca, which are summarized in Table III. As compared to the Fayans EDFs and experiment, the Skyrme models systematically underbind the energies of the hole shells $\pi(1d_{3/2})$ and $\nu(1f_{7/2})$ and underestimate the $Z = 20$ and $N = 28$ shell gaps. Lower separation energies of valence shells and increased quadrupole correlation energies due to smaller shell gaps at $N = 28$ in the Skyrme EDFs result in larger rms charge radii as compared to the Fayans EDFs and experiment. The single-particle energies clearly indicate that the magic nuclei ^{48}Ca and ^{54}Fe are less susceptible to deformation effects in the Fayans models. In the absence of deformation in the Fayans model, which appears to be important for ^{52}Fe in Skyrme models, a nice agreement of

TABLE III. Single-particle energies (MeV) in ^{48}Ca. The DFT values extracted from one-nucleon separation energies as in Ref. [53] are compared to experimental estimates [54].

Orbital	SV-min	UNEDF0	FaNDF^0	DF3-a	Experimental
$\pi(1d_{3/2})$	−14.8	−14.5	−14.8	−15.9	−16.2
$\pi(1f_{7/2})$	−10.6	−10.9	−10.3	−9.7	−9.4
$\nu(1f_{7/2})$	−8.9	−8.6	−9.3	−9.5	−10.0
$\nu(2p_{3/2})$	−6.0	−6.3	−5.3	−5.8	−4.6

the Fayans models with the experiment for $\delta\langle r^2\rangle^{54,52}$ can be attributed to a monopole polarization effect [18].

The rms charge radius generally increases when quadrupole correlations are added to the Skyrme EDFs as seen in Fig. 2. This suggests that a reoptimization of EDFs by including the rms charge radii of Ca and Fe, properly corrected by zero-point fluctuations, could be helpful. In this context, it is noted that a small variation of the saturation density of the Skyrme functional by about 0.002 fm^{-3} would result in a ~0.02 fm change in the rms charge radius [55].

Summary.—Bunched-beam collinear laser spectroscopy was applied for the first time to beams prepared through an in-flight separation followed by a gas stopping. This novel scheme complements the capacity of ISOL facilities and opens new opportunities for laser spectroscopy to explore nuclides far from the stability line. The scheme was demonstrated for neutron deficient ^{52,53}Fe, and the $\delta\nu^{A,A'}$ of the $4s^25D_4 \leftrightarrow 4s4p^5F_5$ transition in Fe I were determined relative to the stable ^{56}Fe. The MCDF method was used to calculate the F_{el} with an estimated error of 15%, which was used to evaluate the k_{SMS} using the King plot analysis. The determined values of $\delta\langle r^2\rangle$ exhibit a sharp minimum at $N = 28$ with $\delta\langle r^2\rangle^{54,52}$ and $\delta\langle r^2\rangle^{54,56}$ being similar. The Fayans-DFT calculations correctly reproduce overall trends of rms charge radii in Fe and Ca isotopes. The main factor appears to be the novel density dependence of the surface energy. Here, further improvements are expected by extending the full Fayans-DFT formalism to deformed shapes [56] and also by adding zero-point multipole correlations. The Skyrme-DFT calculations suggest that the rise of $\delta\langle r^2\rangle^{54,52}$ in Fe is primarily due to deformation effects. On the other hand, since the Ca isotopes are more deformation rigid, the kink at ^{48}Ca is expected to be less impacted by zero-point quadrupole correlations. The poor performance of the Skyrme EDFs in Ca can be traced back to their inability to describe the shell structure of ^{48}Ca [53,57]. The Fayans EDFs with their rich density dependence perform better in predicting the rms charge radii of Ca and Fe. In summary, while the $N = 28$ kinks in Ca and Fe isotopic chains look similar, the underlying mechanisms are different. The unique data on rms charge radii around $N = 28$ in Ca and Fe isotopes will be instrumental for further developments of the nuclear energy density functional.

This work was supported in part by the National Science Foundation, Grant No. PHY-11-02511; the U.S. Department of Energy, National Nuclear Security Administration, Grants No. DE-NA0002924 and No. DE-NA0002847; the U.S. Department of Energy, Office of Science, Office of Nuclear Physics, Grants No. DE-SC0013365, No. DE-AC02-06CH11357, and No. DE-AC05-00OR22725 with UT-Battelle, LLC; the German Research Foundation Contract No. SFB 1245; the German Ministry of Science and Technology, Grants No. 05P12RFFTG and No. 015P15SJCIA; the Russian Science Foundation, Grants No. 16-12-10155 and No. 16-12-10161 and the RFBR Grants No. 14-02-00107-a, No. 14-22-03040-ofi_m, and No. 16-02-00228-a. Calculations were partially carried out at the Computer Center of Kurchatov Institute.

[1] H. Geiger and E. Marsden, Proc. R. Soc. A **82**, 495 (1909).
[2] E. Rutherford, Philos. Mag. **21**, 669 (1911).
[3] E. W. Otten, *Treatise on Heavy Ion Science* (Springer, New York, 1989), pp. 517–638.
[4] H. J. Kluge and W. Nörtershäuser, Spectrochim. Acta B Atom. Spectros. **58**, 1031 (2003).
[5] B. Cheal and K. T. Flanagan, J. Phys. G **37**, 113101 (2010).
[6] K. Blaum, J. Dilling, and W. Nörtershäuser, Phys. Scr. T **T152**, 014017 (2013).
[7] P. Campbell, I. D. Moore, and M. R. Pearson, Prog. Part. Nucl. Phys. **86**, 127 (2016).
[8] D. J. Morrissey, B. M. Sherrill, M. Steiner, A. Stolz, and I. Wiedenhoever, Nucl. Instrum. Methods Phys. Res., Sect. B **204**, 90 (2003).
[9] K. Cooper, C. Sumithrarachchi, D. Morrissey, A. Levand, J. Rodriguez, G. Savard, S. Schwarz, and B. Zabransky, Nucl. Instrum. Methods Phys. Res., Sect. A **763**, 543 (2014).
[10] I. Angeli and K. P. Marinova, At. Data Nucl. Data Tables **99**, 69 (2013).
[11] P.-G. Reinhard and H. Flocard, Nucl. Phys. **A584**, 467 (1995).
[12] M. Bender, G. F. Bertsch, and P.-H. Heenen, Phys. Rev. C **73**, 034322 (2006).
[13] H. DeWitte *et al.*, Phys. Rev. Lett. **98**, 112502 (2007).
[14] P. M. Goddard, P. D. Stevenson, and A. Rios, Phys. Rev. Lett. **110**, 032503 (2013).
[15] D. M. Rossi, K. Minamisono, H. B. Asberry, G. Bollen, B. A. Brown, K. Cooper, B. Isherwood, P. F. Mantica, A. Miller, D. J. Morrissey, R. Ringle, J. A. Rodriguez, C. A. Ryder, A. Smith, R. Strum, and C. Sumithrarachchi, Phys. Rev. C **92**, 014305 (2015).
[16] H. Nakada and T. Inakura, Phys. Rev. C **91**, 021302 (2015).
[17] H. Nakada, Phys. Rev. C **92**, 044307 (2015).
[18] S. A. Fayans, S. V. Tolokonnikov, E. L. Trykov, and D. Zawischa, Nucl. Phys. **A676**, 49 (2000).
[19] S. V. Tolokonnikov and E. E. Saperstein, Phys. At. Nucl. **73**, 1684 (2010).
[20] G. Hagen, A. Ekstrom, C. Forssen, G. R. Jansen, W. Nazarewicz, T. Papenbrock, K. A. Wendt, S. Bacca, N. Barnea, B. Carlsson, C. Drischler, K. Hebeler, M. Hjorth-Jensen, M. Miorelli, G. Orlandini, A. Schwenk, and J. Simonis, Nat. Phys. **12**, 186 (2016).
[21] R. F. G. Ruiz *et al.*, Nat. Phys. **12**, 594 (2016).
[22] F. C. Charlwood, J. Billows, P. Campbell, B. Cheal, T. Eronen, D. H. Forest, S. Fritzsche, M. Honma, A. Jokinen, I. D. Moore, H. Penttilä, R. Powis, A. Saastamoinen, G. Tungate, and J. Äystö, Phys. Lett. B **690**, 346 (2010).
[23] K. Minamisono, P. F. Mantica, A. Klose, S. Vinnikova, A. Schneider, B. Johnson, and B. R. Barquest, Nucl. Instrum. Methods Phys. Res., Sect. A **709**, 85 (2013).
[24] D. M. Rossi, K. Minamisono, B. R. Barquest, G. Bollen, K. Cooper, M. Davis, K. Hammerton, M. Hughes, P. F.

Mantica, D. J. Morrissey, R. Ringle, J. A. Rodriguez, C. A. Ryder, S. Schwarz, R. Strum, C. Sumithrarachchi, D. Tarazona, and S. Zhao, Rev. Sci. Instrum. **85**, 093503 (2014).
[25] B. R. Barquest, Ph.D. thesis, Michigan State University, 2014.
[26] P. Campbell, H. L. Thayer, J. Billowes, P. Dendooven, K. T. Flanagan, D. H. Forest, J. A. R. Griffith, J. Huikari, A. Jokinen, R. Moore, A. Nieminen, G. Tungate, S. Zemlyanoi, and J.Äystö, Phys. Rev. Lett. **89**, 082501 (2002).
[27] A. Nieminen, P. Campbell, J. Billowes, D. H. Forest, J. A. R. Griffith, J. Huikari, A. Jokinen, I. D. Moore, R. Moore, G. Tungate, and J. Äystö, Phys. Rev. Lett. **88**, 094801 (2002).
[28] A. Klose, K. Minamisono, C. Geppert, N. Frömmgen, M. Hammen, J. Krämer, A. Krieger, C. D. P. Levy, P. F. Mantica, W. Nörtershäuser, and S. Vinnikova, Nucl. Instrum. Methods Phys. Res., Sect. A **678**, 114 (2012).
[29] C. A. Ryder, K. Minamisono, H. B. Asberry, B. Isherwood, P. F. Mantica, A. Miller, D. M. Rossi, and R. Strum, Spectrochim. Acta Part B **113**, 16 (2015).
[30] T. R. O'Brian, M. E. Wickliffe, J. E. Lawler, W. Whaling, and J. W. Brault, J. Opt. Soc. Am. B **8**, 1185 (1991).
[31] A. Klose, K. Minamisono, and P. F. Mantica, Phys. Rev. A **88**, 042701 (2013).
[32] I. P. Grant, *Relativistic Quantum Theory of Atoms and Molecules: Theory and Computation* (Springer, New York, 2007), Vol. 40.
[33] P. Jönsson, X. He, C. F. Fischer, and I. P. Grant, Comput. Phys. Commun. **177**, 597 (2007).
[34] C. Nazé, E. Gaidamauskas, G. Gaigalas, M. Godefroid, and P. Jönsson, Comput. Phys. Commun. **184**, 2187 (2013).
[35] B. Cheal, T. E. Cocolios, and S. Fritzsche, Phys. Rev. A **86**, 042501 (2012).
[36] S. Fritzsche, C. F. Fischer, and G. Gaigalas, Comput. Phys. Commun. **148**, 103 (2002).
[37] S. Krins, S. Oppel, N. Huet, J. vonZanthier, and T. Bastin, Phys. Rev. A **80**, 062508 (2009).
[38] S. G. Porsev, M. G. Kozlov, and D. Reimers, Phys. Rev. A **79**, 032519 (2009).
[39] W. King, *Isotope Shifts in Atomic Spectra* (Plenum, New York, 1984).
[40] G. Fricke and K. Heilig, *Nuclear Charge Radii* (Springer, Berlin, 2004).
[41] R. C. Barrett, Phys. Lett. **33B**, 388 (1970).
[42] M. Bender, P.-H. Heenen, and P.-G. Reinhard, Rev. Mod. Phys. **75**, 121 (2003).
[43] P. Klüpfel, P.-G. Reinhard, T. J. Bürvenich, and J. A. Maruhn, Phys. Rev. C **79**, 034310 (2009).
[44] M. Kortelainen, T. Lesinski, J. Moré, W. Nazarewicz, J. Sarich, N. Schunck, M. V. Stoitsov, and S. Wild, Phys. Rev. C **82**, 024313 (2010).
[45] S. A. Fayans, JETP Lett. **68**, 169 (1998).
[46] J. Dobaczewski, W. Nazarewicz, and M. V. Stoitsov, Eur. Phys. J. A **15**, 21 (2002).
[47] P. G. Reinhard and K. Goeke, Rep. Prog. Phys. **50**, 1 (1987).
[48] J. Erler, P. Klüpfel, and P.-G. Reinhard, J. Phys. G **38**, 033101 (2011).
[49] L. Vermeeren, P. Lievens, R. E. Silverans, U. Georg, M. Keim, A. Klein, R. Neugart, M. Neuroth, and F. Buchinger (the ISOLDE Collaboration), J. Phys. G **22**, 1517 (1996).
[50] P. Campbell, A. Nieminen, J. Billowes, P. Dendooven, K. T. Flanagan, D. H. Forest, Y. P. Gangrsky, J. A. R. Griffith, J. Juikari, A. Jokinen, I. D. Moore, R. Moore, H. L. Thayer, G. Tungate, S. G. Zemlyanoi, and J.Äystö, Eur. J. Phys. A **15**, 45 (2002).
[51] K. Kreim, M. L. Bissell, J. Papuga, K. Blaum, M. D. Rydt, R. F. G. Ruiz, S. Goriely, H. Heylen, M. Kowalska, R. Neugart, G. Neyens, W. Nörtershäuser, M. M. Rajabali, R. S. Alarcon, H. H. Stroke, and D. T. Yordanov, Phys. Lett. B **731**, 97 (2014).
[52] K. L. Yurkewicz, D. Bazin, B. A. Brown, C. M. Campbell, J. A. Church, D. C. Dinca, A. Gade, T. Glasmacher, M. Honma, T. Mizusaki, W. F. Muller, H. Olliver, T. Otsuka, L. A. Riley, and J. R. Terry, Phys. Rev. C **70**, 034301 (2004).
[53] M. Kortelainen, J. McDonnell, W. Nazarewicz, E. Olsen, P.-G. Reinhard, J. Sarich, N. Schunck, S. M. Wild, D. Davesne, J. Erler, and A. Pastore, Phys. Rev. C **89**, 054314 (2014).
[54] N. Schwierz, I. Wiedenhover, and A. Volya, arXiv: 0709.3525.
[55] P.-G. Reinhard and W. Nazarewicz, Phys. Rev. C **93**, 051303 (2016).
[56] S. V. Tolokonnikov, I. N. Borzov, M. Kortelainen, Y. S. Lutostansky, and E. E. Saperstein, J. Phys. G **42**, 075102 (2015).
[57] D. Tarpanov, J. Dobaczewski, J. Toivanen, and B. G. Carlsson, Phys. Rev. Lett. **113**, 252501 (2014).